Inorg. Chem. **2005**, *44*, 122–132

Reactions of Potent Antitumor Complex *trans*-$[Ru^{III}Cl_4(indazole)_2]^-$ with a DNA-Relevant Nucleobase and Thioethers: Insight into Biological Action

Alexander Egger,[†] Vladimir B. Arion,*[,†] Erwin Reisner,[†] Berta Cebrián-Losantos,[†] Sergiu Shova,[‡] Günter Trettenhahn,[§] and Bernhard K. Keppler*[,†]

Institute of Inorganic Chemistry of the University of Vienna, Währingerstrasse 42, A-1090 Vienna, Austria, Institute of Physical Chemistry of the University of Vienna, Währingerstrasse 42, A-1090 Vienna, Austria, and Department of Chemistry, Moldova State University, A. Mateevici Street 60, 2009 Chisinau, Moldova

Received July 30, 2004

Reactions of the complex *trans*-$[RuCl_4(Hind)_2]^-$ (Hind = indazole), which is of clinical relevance today, with both the DNA model nucleobase 9-methyladenine (made) and the thioethers R_2S (R = Me, Et), as models of the methionine residue in biological molecules possibly acting as nitrogen-competing sulfur-donor ligands for ruthenium atom, have been investigated to get insight into details of mechanism leading to antitumor activity. Three novel ruthenium complexes, viz., $[Ru^{III}Cl_3(Hind)_2(made)]$, **1**, $[Ru^{II}Cl_2(Hind)_2(Me_2S)_2]$, **2**, and $[Ru^{II}Cl_2(Hind)_2(Et_2S)_2]$, **3**, have been isolated as solids. Oxidation of **2** and **3** with hydrogen peroxide in the presence of 12 M HCl in chloroform afforded the monothioether adducts, viz., $[Ru^{III}Cl_3(Hind)_2(Me_2S)]$, **4**, and $[Ru^{III}Cl_3(Hind)_2(Et_2S)]$, **5**. By dissolution of **2** or **3** in DMSO, replacement of both R_2S ligands by DMSO molecules occurred with isolation of *trans*,*trans*,*trans*-$[Ru^{II}Cl_2(Hind)_2(DMSO)_2]$, **6**. The products were characterized by elemental analysis, IR, UV–vis, electrospray mass spectrometry, cyclic voltammetry, and X-ray crystallography (**1**·CH_2Cl_2·CH_3OH and **1**·$1.1H_2O$·$0.9CH_3OH$, **2**, and **5**). The first crystallographic evidence for the monofunctional coordination of the 9-methyladenine ligand to ruthenium via N7 and the self-pairing of the complex molecules via H-bonding, using the usual Watson–Crick pairing donor and acceptor sites of two adjacent 9-methyladenine ligands, is reported. The electrochemical behavior of **1**–**5** has been studied in DMF and DMSO by cyclic voltammetry. The redox potential values have been interpreted on the basis of the Lever's parametrization method. The E_L parameter was estimated for 9-methyladenine at 0.18 V, showing that this ligand behaves as a weaker net electron donor than imidazole (E_L = 0.12 V). The kinetics of the reductively induced stepwise replacement of chlorides by DMF in **4** and **5** were studied by digital simulation of the cyclic voltammograms. The rate constant k_1 has been determined as 0.9 ± 0.1 s^{-1}, which obeys the first-order rate law, while k_2 is concentration dependent (0.2 ± 0.1 $M^{1-n}\cdot s^{-1}$ with $n > 1$ for 4 mM solutions of **4** and **5**), indicating higher-order reactions mechanism.

Introduction

The potential of ruthenium coordination and organometallic compounds for the development of antitumor drugs is well recognized.[1–9] Two ruthenium(III) complexes (H_2im)[*trans*-$Ru^{III}Cl_4$(Him)(DMSO)] (NAMI-A; Him = imidazole)[10] and (H_2ind)[*trans*-$Ru^{III}Cl_4(Hind)_2$] (KP1019; Hind = indazole)[8] have entered phase I clinical trials, the first as an

* Authors to whom correspondence should be addressed. E-mail: arion@ap.univie.ac.at (V.B.A.); keppler@ap.univie.ac.at (B.K.K.). Fax: +43 1 427752680 (both).

[†] Institute of Inorganic Chemistry, University of Vienna.

[‡] Moldova State University.

[§] Institute of Physical Chemistry, University of Vienna.

(1) (a) Clarke, M. J.; Zhu, F.; Frasca, D. R. *Chem. Rev.* **1999**, *99*, 2511–2533. (b) Clarke, M. J. Coord. Chem. Rev. **2003**, *236*, 209–233.

(2) (a) Guo, Z.; Sadler, P. J. *Angew. Chem., Int. Ed.* **1999**, *38*, 1512–1531. (b) Morris, R. E.; Aird, R. E.; Murdoch, P. del S.; Chen, H.; Cummings, J.; Hughes, N. D.; Parsons, S.; Parkin, A.; Boyd, G.; Jodrell, D. I.; Sadler, P. J. *J. Med. Chem.* **2001**, *44*, 3616–3621.

(3) Alessio, E.; Mestroni, G.; Nardin, G.; Attia, W. M.; Calligaris, M.; Sava, G.; Zorzet, S. *Inorg. Chem.* **1988**, *27*, 4099–4106.

(4) Velders, A. H.; Kooijman, H.; Spek, A. L.; Haasnoot, J. G.; De Vos, D.; Reedijk, J. *Inorg. Chem.* **2000**, *39*, 2966–2967.

(5) Vilaplana, R. A.; Gonzalez-Vilchez, F.; Gutierrez-Puebla, E.; Ruiz-Valero, C. *Inorg. Chim. Acta* **1994**, *224*, 15–18.

10.1021/ic048967h CCC: $30.25
Published on Web 12/08/2004

antimetastatic drug and the second as an anticancer agent against primary tumors and metastases and, in particular, colon carcinomas. Despite the plethora of biological investigations both in vitro and in vivo,[11] the mode of action of these compounds at a molecular level is largely not understood and of much interest.[12] As for a number of other antitumor ruthenium compounds,[13] the potential target for *trans*-[RuCl$_4$(Hind)$_2$]$^-$ is DNA.[12c] A recent capillary electrophoresis study on the binding of (H$_2$ind)[*trans*-RuCl$_4$(Hind)$_2$] with all four DNA-relevant nucleoside monophosphates in buffered solution showed a preference for GMP and AMP coordination,[14] although the actual metal-binding sites have not yet been established. An investigation of interactions of KP1019 with purine bases protected at the sugar position 9 by alkyl substituents seems to be necessary to elucidate its potential modes of binding with GMP and AMP as part of a large scale effort to establish the DNA binding sites.

Although DNA appears to be an important target site for the compounds exhibiting cytotoxic activity, the intravenously administered metallodrug has to follow a long route to reach the cell. An understanding of the mechanism of action of metallo(pro)drugs also requires the study of their interactions with other possible biological targets present in blood plasma, in the cell membrane, or in the cytoplasm, which can act as competing ligands, e.g., amino acids, peptides, proteins, hormones, etc.[15] The interaction of sulfur-donor ligands with the metal seems to be of major relevance in this case because of their strong affinity for ruthenium.

This prompted us to study the reactions of *trans*-[RuCl$_4$(Hind)$_2$]$^-$ with both a DNA-relevant nucleobase, viz., 9-methyladenine, and thioethers to model the binding of nitrogen- and sulfur-containing residues in biomolecules to ruthenium via Ru−ligand exchange reactions. We show in this paper that both 9-methyladenine and thioethers are capable of substituting chloro ligand(s) at the six-coordinate ruthenium center. This implies the potential ability of methionine residues to act as nitrogen-competing ligands for binding to *trans*-[RuCl$_4$(Hind)$_2$]$^-$. Reactions of the latter with prepared 9-methyladenine and thioethers R$_2$S, with R = Me and Et, afforded three novel complexes, viz., *mer*,*trans*-[Ru^{III}Cl$_3$(Hind)$_2$(made)] (**1**), *trans*,*trans*,*trans*-[Ru^{II}Cl$_2$(Hind)$_2$(Me$_2$S)$_2$] (**2**), and *trans*,*trans*,*trans*-[Ru^{II}Cl$_2$(Hind)$_2$(Et$_2$S)$_2$] (**3**) (Scheme 1). The first crystallographic evidence for monofunctional binding of 9-substituted adenine to ruthenium via N7 is presented. This mode of attachment is somewhat surprising since coordination through more basic N1 site might be expected under the experimental conditions. The isolated thioether adducts **2** and **3** are able to release one of the two thioether ligands on oxidation, yielding the ruthenium(III) species *mer*,*trans*-[Ru^{III}Cl$_3$(Hind)$_2$(Me$_2$S)] (**4**) and *mer*,*trans*-[Ru^{III}Cl$_3$(Hind)$_2$(Et$_2$S)] (**5**). Replacement of thioether ligands of **2** and **3** by DMSO molecules with retention of complex configuration and isolation of [RuCl$_2$(Hind)$_2$(DMSO)$_2$] can be easily performed. A detailed study of the electrochemical behavior of **1**−**5** is also reported.

Experimental Section

Hydrated RuCl$_3$ purchased from Degussa and dimethyl sulfide and diethyl sulfide from Aldrich were used as received. 9-Methyladenine (made)[16,17] and [NMe$_4$][*trans*-Ru^{III}Cl$_4$(Hind)$_2$][18] were prepared as reported elsewhere.

Synthesis of Complexes. *mer*,*trans*-[Trichlorobis(indazole)(9-methyladenine)ruthenium(III)], [Ru^{III}Cl$_3$(Hind)$_2$(made)] (1). A solution of [NMe$_4$][*trans*-Ru^{III}Cl$_4$(Hind)$_2$] (0.11 g, 0.2 mmol) and 9-methyladenine (0.06 g, 0.4 mmol) in ethanol (15 mL) was stirred under reflux for 1 h. The solvent of the deep-red solution formed was removed by rotary evaporation under reduced pressure. The solid residue was extracted with CHCl$_3$/MeOH (10:1) and then purified by column chromatography on silica by using as eluent a mixture of CH$_2$Cl$_2$/CH$_3$CN (5:2). Yield: 0.04 g, 15%. The complex was well soluble in chloroform and DMF and less soluble in methanol. Anal. Calcd for C$_{20}$H$_{19}$N$_9$Cl$_3$Ru·1/3CHCl$_3$ (M_r = 592.85 g/mol): C, 38.60; H, 3.08; N 19.93; Cl, 22.44. Found: C, 38.67; H, 2.96; N, 19.73; Cl, 22.04. ESI-MS(positive), *m*/*z* (% rel int): 557 (100), [Ru^{III}Cl$_2$(Hind)$_2$(made)]$^+$; 150 (25), [Hmade]$^+$. ESI-MS(negative), *m*/*z* (% rel int): 629 (40), [RuCl$_3$(Hind)$_2$(made) + Cl]$^-$; 593 (100), [RuCl$_3$(Hind)$_2$(made) − H]$^-$; 480 (65), [RuCl$_4$(Hind)$_2$]$^-$; 326 (25), [RuCl$_3$(ind)]$^-$. IR spectrum in KBr, selected bands, cm^{-1}: 3330 s, ν(NH); 1662 vs; 1627 s; 1591 vs; 1356 s; 1237 s; 745 s. UV−vis (methanol), λ_{max}, nm (ϵ, M^{-1} cm^{-1}): 380 (3300), 428 (2030). X-ray diffraction quality rectangular plates and

(6) Allardyce, C. S.; Dyson, P. J. *Platinum Met. Rev.* **2001**, *45*, 62−69.
(7) Jaswal, J. S.; Rettig, S. J.; James, B. R. *Can. J. Chem.* **1990**, *68*, 1808−1817.
(8) Galanski, M.; Arion, V. B.; Jakupec, M. A.; Keppler, B. K. *Curr. Pharm. Des.* **2003**, *9*, 2078−2089.
(9) Mura, P.; Camalli, M.; Messori, L.; Piccioli, F.; Zanello, P.; Corsini, M. *Inorg. Chem.* **2004**, *43*, 3863−3870.
(10) Sava, G.; Gagliardi, R.; Bergamo, A.; Alessio, E.; Mestroni, G. *Anticancer Res.* **1999**, *19*, 969−972.
(11) (a) Sava, G.; Pacor, S.; Zorzet, S.; Alessio, E.; Mestroni, G. *Pharmacol. Res.* **1989**, *21*, 617−628. (b) Alessio, E.; Xu, Y.; Cauci, S.; Mestroni, G.; Quadrifoglio, F.; Viglino, P.; Marzilli, L. G. *J. Am. Chem. Soc.* **1989**, *111*, 7068−7071. (c) Hotze, A. C. G.; Velders, A. H.; Ugozzoli, F.; Biagini-Cingi, M.; Manotti-Lanfredi, A. M.; Haasnoot, J. C.; Reedijk, J. *Inorg. Chem.* **2000**, *39*, 3838−3844.
(12) (a) Wang, F.; Chen, H.; Parkinson, J. A.; Murdoch, P. del S.; Sadler, P. J. *Inorg. Chem.* **2002**, *41*, 4509−4523. (b) Pongratz, M.; Schluga, P.; Jakupec, M. A.; Arion, V. B.; Hartinger, C. G.; Allmaier, G.; Keppler, B. K. *J. Anal. At. Spektrom.* **2004**, *19*, 46−51. (c) Malina, J.; Novakova, O.; Keppler, B. K.; Alessio, E.; Brabec, V. *J. Biol. Inorg. Chem.* **2001**, *6*, 435−445.
(13) (a) Frasca, D.; Ciampa, J.; Emerson, J.; Umans, R. S.; Clarke, M. J. *Met.-Based Drugs* **1996**, *3*, 197−209. (b) Carballo, M.; Vilaplana, R.; Marquez, G.; Conde, M.; Bedoya, F. J.; Gonzalez-Vilchez, F.; Sobrino, F. *Biochem. J.* **1997**, *328*, 559−564. (c) Van Vliet, P. M.; Toekimin, S. M. S.; Sarinten, M. S.; Haasnoot, J. G.; Reedijk, J.; Nováková, O.; Vrána, O.; Brabec, V. *Inorg. Chim. Acta* **1995**, *231*, 57−64. (d) Messori, L.; Orioli, P.; Vullo, D.; Alessio, E.; Iengo, E. *Eur. J. Biochem.* **2000**, *267*, 1206−1213. (e) Kratz, F. In *Metal Complexes in Cancer Chemotherapy*; Keppler, B. K., Ed.; VCH: Weinheim, Germany, 1993; pp 391−429. (f) Keppler, B. K., Lipponer, K. G., Stenzel, B.; Kratz, F. *Metal Complexes in Cancer Chemotherapy*; Keppler, B. K., Ed.; VCH: Weinheim, Germany, 1993; pp 187−220.
(14) Küng, A.; Pieper, T.; Keppler, B. K. *J. Chromatogr., B* **2001**, *759*, 81−89.
(15) (a) Kratochwil, N. A.; Guo, Z.; Murdoch, P.-d. S.; Parkinson, J. A.; Bednarski, P. J.; Sadler, P. J. *J. Am. Chem. Soc.* **1998**, *120*, 8253−8254. (b) Mestroni, G.; Alessio, E.; Sava, G.; Pacor, S.; Coluccia, M.; Boccarelli, A. *Met.-Based Drugs* **1994**, *1*, 41−63. (c) Clarke, M. J.; Bitler, S.; Rennert, D.; Buchbinder, M.; Kelman, A. D. *J. Inorg. Biochem.* **1980**, *12*, 79−87.
(16) Talman, E. G.; Bruening, W.; Reedijk, J.; Spek, A. L.; Veldman, N. *Inorg. Chem.* **1997**, *36*, 854−861.
(17) Charland, J. P.; Phan Viet, M. T.; St-Jacques, M.; Beauchamp, A. L. *J. Am. Chem. Soc.* **1985**, *107*, 8202−8211.
(18) Peti, W.; Pieper, T.; Sommer, M.; Keppler, B. K.; Giester, G. *Eur. J. Inorg. Chem.* **1999**, 1551−1555.

Scheme 1. Synthetic Pathways to Complexes **1**−**6**

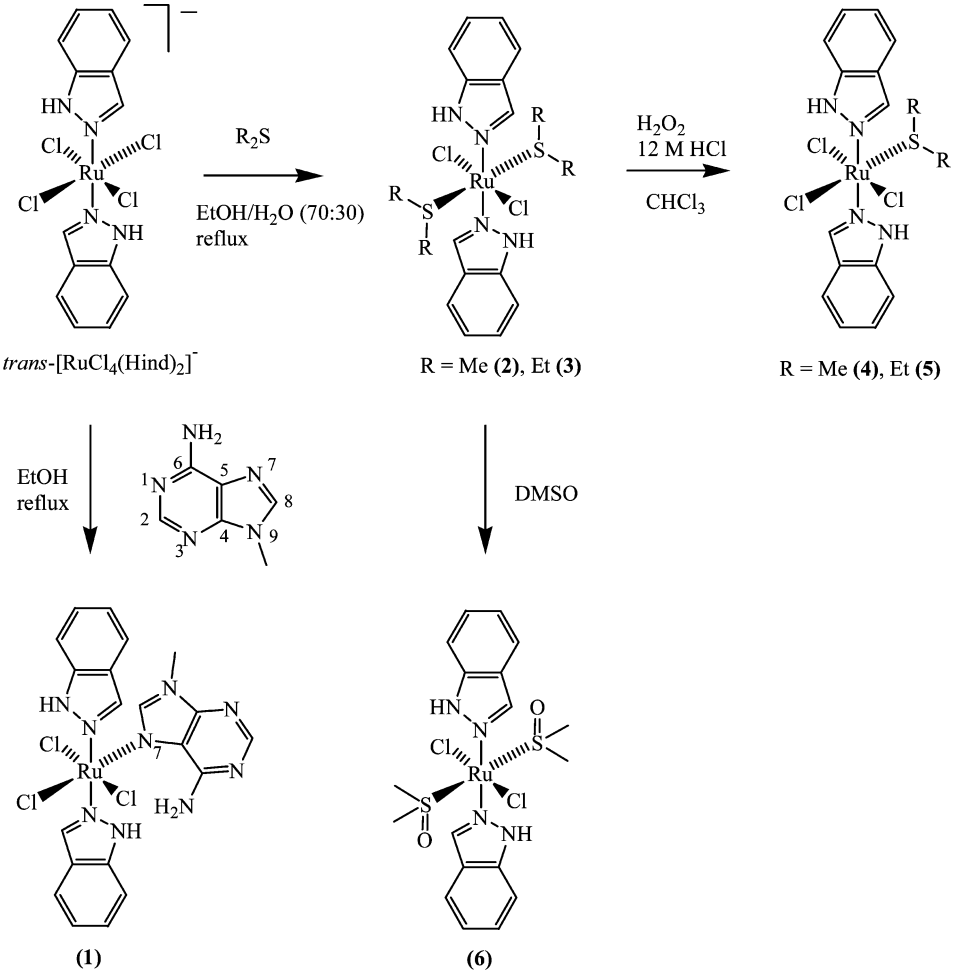

needlelike crystals were grown by slow diffusion of hexane into a dichloromethane solution of **1**, containing a few drops of methanol.

***trans*,*trans*,*trans*-[Dichlorobis(dimethyl sulfide)bis(indazole)-ruthenium(II)], [$Ru^{II}Cl_2(Hind)_2(Me_2S)_2$] (2).** Dimethyl sulfide (2.5 mL) was added to a solution of [NMe_4][*trans*-$Ru^{III}Cl_4(Hind)_2$] (0.55 g, 1.0 mmol) in 70:30 ethanol/water (v/v) (200 mL) and the reaction mixture refluxed at 90 °C for 2 h. The color of the solution changed at the beginning from orange to deep red and at the end of the reaction to green. The solution was allowed to cool to room temperature yielding yellow-orange needles of X-ray diffraction quality, which were separated by filtration, washed with 70:30 ethanol/water, and dried in air. Yield: 0.26 g, 48%. The complex was well soluble in chloroform, DMSO, and DMF and insoluble in methanol, ethanol, and water. Anal. Calcd for $C_{18}H_{24}N_4Cl_2RuS_2$ (M_r = 532.52 g/mol): C, 40.60; H, 4.54; N 10.52; Cl, 13.32; S, 12.04. Found: C, 40.49; H, 4.55; N, 10.59; Cl, 13.23; S, 11.94. ESI-MS(positive), *m*/*z* (% rel int): 532 (100), $[Ru^{III}Cl_2(Hind)_2(Me_2S)_2]^+$; 497 (80), $[Ru^{II}Cl(Hind)_2(Me_2S)_2]^+$. IR spectrum in KBr, selected bands, cm^{-1}: 3273 s; ν(NH); 1355 vs; 686 vs UV−vis ($CHCl_3$), λ_{max}, nm (ϵ, M^{-1} cm^{-1}): 293 (6810), 361 (12590). ^1H NMR in $CDCl_3$ (δ, ppm): 12.23 (s, 2H, N*H*), 8.92 (s, 2H, C*H* = N), 7.74 (d, 2H, ArH, J = 8.1 Hz), 7.50 (d, 2H, ArH, J = 8.3 Hz), 7.42 (t, 2H, ArH, J = 7.0 Hz), 7.22 (t, 2H, ArH, J = 7.4 Hz), 1.87 (s, 12H, $(CH_3)_2S$). $^{13}C\{^1H\}$ NMR in $CDCl_3$ (δ, ppm): 140.8, 139.9, 127.6, 124.0, 121.9, 120.2, 109.5, 20.4.

***trans*,*trans*,*trans*-[Dichlorobis(diethyl sulfide)bis(indazole)ruthenium(II)], [$Ru^{II}Cl_2(Hind)_2(Et_2S)_2$] (3).** Diethyl sulfide (0.5 mL) was added to a solution of [NMe_4][*trans*-$Ru^{III}Cl_4(Hind)_2$] (0.11 g, 0.2 mmol) in 70:30 ethanol/water (v/v) (40 mL) and the reaction mixture heated at 80 °C for 1 h. The light-green solution, from which some amount of a fine yellow powder precipitated already after 15 min of heating, was allowed to cool to room temperature. The product was filtered off, washed with 70:30 ethanol/water, and dried in a vacuum. Yield: 0.09 g, 75%. The complex was well soluble in chloroform, DMSO, and DMF and insoluble in methanol, ethanol, and water. Anal. Calcd for $C_{22}H_{32}N_4Cl_2RuS_2$ (M_r = 588.62 g/mol): C, 44.89; H, 5.48; N 9.52; Cl, 12.05; S, 10.89. Found: C, 44.92; H, 5.57; N, 9.54; Cl, 11.99; S, 10.83. ESI-MS(positive), *m*/*z* (% rel int): 408 (100), $[Ru^{III}Cl_2(Hind)_2]^+$; 498 (70), $[Ru^{III}Cl_2(Hind)_2(Et_2S)]^+$. IR spectrum in KBr, selected bands, cm^{-1}: 3266 s, ν(NH); 1352 vs; 692 vs UV−vis ($CHCl_3$), λ_{max}, nm (ϵ, M^{-1} cm^{-1}): 297 (6750), 369 (14300). ^1H NMR in $CDCl_3$; (δ, ppm): 12.23 (s, 2H, N*H*), 8.90 (s, 2H, C*H* = N), 7.71 (d, 2H, ArH, J = 8.1 Hz), 7.50 (d, 2H, ArH, J = 8.5 Hz), 7.41 (t, 2H, ArH, J = 7.5 Hz), 7.21 (t, 2H, ArH, J = 7.5 Hz), 2.42 (q, 8H, $(CH_3CH_2)_2S$, J = 7.4 Hz), 1.01 (t, 12H, $(CH_3CH_2)_2S$, J = 7.4 Hz). $^{13}C\{^1H\}$ NMR in $CDCl_3$ (δ, ppm): 140.8, 140.1, 127.4, 124.3, 121.7, 120.1, 109.4, 27.1, 13.5.

***mer*,*trans*-[Trichloro(dimethyl sulfide)bis(indazole)ruthenium(III)], [$Ru^{III}Cl_3(Hind)_2(Me_2S)$] (4).** The 12 M HCl (0.05 mL) and hydrogen peroxide (30%) (0.02 mL) were added to a yellow-orange solution of **2** (0.06 g, 0.1 mmol) in chloroform (30 mL), and the reaction mixture was stirred at 50 °C for 2 h. A small quantity of green precipitate formed was separated by filtration and thrown away. The solvent was further removed by rotary evaporation under reduced pressure and the solid residue recrystallized from

Table 1. Crystal Data and Details of Data Collection for **1a**,**b**, **2**, and **5**

param	**1a**	**1b**	**2**	**5**
empirical formula	$C_{22}H_{25}N_9RuCl_5O$	$C_{21}H_{24.6}N_9RuCl_3O$	$C_{18}H_{24}N_4RuCl_2S_2$	$C_{18}H_{22}N_4RuCl_3S$
fw	709.83	642.52	532.50	533.88
space group	$P\bar{1}$	$P2_1/n$	$C2/c$	$P2_1/c$
a, Å	9.486(2)	14.834(3)	15.725(3)	17.029(3)
b, Å	11.427(2)	9.763(2)	9.883(2)	12.393(2)
c, Å	13.972(3)	18.102(4)	14.080(3)	20.013(4)
α, deg	102.31(3)			
β, deg	98.72(3)	100.33(3)	102.39(3)	90.91(3)
γ, deg	98.82(3)			
V, Å^3	1435.3(5)	2579.1(9)	2137.2(7)	4223.0(13)
Z	2	4	4	8
λ, Å	0.710 73	0.710 73	0.710 73	0.710 73
ρ_{calcd}, g cm^{-3}	1.642	1.655	1.655	1.679
cryst size, mm^3	0.23 × 0.23 × 0.11	0.14 × 0.09 × 0.06	0.14 × 0.06 × 0.05	0.34 × 0.34 × 0.29
T, K	120	120	120	120
μ, cm^{-1}	10.46	9.57	11.90	12.32
R1[a]	0.0362	0.0261	0.0391	0.0600
wR2[b]	0.0880	0.0632	0.0886	0.1753
GOF[c]	1.023	1.033	0.998	1.080

[a] $R1 = \sum||F_o| - |F_c||/\sum|F_o|$. [b] $wR2 = \{\sum[w(F_o^2 - F_c^2)^2]/\sum[w(F_o^2)^2]\}^{1/2}$. [c] $GOF = \{\sum[w(F_o^2 - F_c^2)^2]/(n - p)\}^{1/2}$, where n is the number of reflections and p is the total number of parameters refined.

methanol (15 mL). The brown crystals were separated by filtration and dried in a vacuum. Yield: 0.01 g, 20%. The complex was well soluble in chloroform and less soluble in methanol and ethanol. Anal. Calcd for $C_{16}H_{18}N_4Cl_3RuS$ (M_r = 505.83 g/mol): C, 37.99; H, 3.59; N 11.08; S, 6.34. Found: C, 37.90; H, 3.53; N, 10.79; S, 6.24. ESI-MS(positive), *m*/*z* (% rel int): 532 (100), $[Ru^{III}Cl_2(Hind)_2(Me_2S)_2]^+$; 470 (30), $[Ru^{III}Cl_2(Hind)_2(Me_2S)]^+$; 408 (30) $[Ru^{III}Cl_2(Hind)_2]^+$. IR spectrum in KBr, selected bands, cm^{-1}: 1356 vs; 747 vs. UV−vis ($CHCl_3$), λ_{max}, nm (ϵ, M^{-1} cm^{-1}): 286 (17450), 366 (3800), 444 (1850).

***mer*,*trans*-[Trichloro(diethyl sulfide)bis(indazole)ruthenium-(III)], [Ru^{III}Cl$_3$(Hind)$_2$(Et$_2$S)] (5).** The 12 M HCl (0.03 mL) and hydrogen peroxide (30%) (0.03 mL) were added to a yellow-orange solution of **3** (0.09 g, 0.15 mmol) in chloroform (30 mL), and the reaction mixture was stirred at 50 °C for 1.5 h. The red solution was allowed to cool to room temperature, and the solvent was removed by rotary evaporation under reduced pressure. The product was dried in a vacuum. Yield: 0.06 g, 76%. The complex is well soluble in chloroform and less soluble in methanol and ethanol. Anal. Calcd for $C_{18}H_{22}N_4Cl_3RuS$ (M_r = 533.89 g/mol): C, 40.50; H, 4.15; N 10.49; S, 6.01. Found: C, 40.59; H, 4.09; N, 10.12; S, 6.02. ESI-MS(positive), *m*/*z*: 498 (100%), $[Ru^{III}Cl_2(Hind)_2(Et_2S)]^+$. IR spectrum in KBr, selected bands, cm^{-1}: 1355 vs; 747 vs. UV−vis ($CHCl_3$), λ_{max}, nm (ϵ, M^{-1} cm^{-1}): 287 (23850), 384 (3620), 446 (2760). X-ray diffraction quality crystals have been obtained by slow vapor diffusion of pentane into chloroform solution of **5**.

***trans*,*trans*,*trans*-[Dichlorobis(dimethyl sulfoxide)bis(indazole)ruthenium(II)], *trans*,*trans*,*trans*-[RuCl$_2$(Hind)$_2$(DM*S*O)$_2$] (6).** A solution of **3** (0.04 g, 0.07 mmol) in DMSO (20 mL) was allowed to stand at room temperature. After 5 h yellow microcrystalline plates started to form. They were filtered off after 5 days, washed with methanol and diethyl ether, and dried in a vacuum. Yield: 0.03 g, 78%. Anal. Calcd for $C_{18}H_{24}Cl_2N_4O_2RuS_2$ (M_r = 564.52 g/mol): C, 38.30; H, 4.29; N, 9.92; Cl, 12.56; S, 11.36. Found: C, 38.08; H, 4.32; N, 9.75; Cl, 12.10; S, 11.39. IR spectrum in KBr, selected bands, cm^{-1}: 3249 s, ν(N−H); 3008 s; 2925 m, ν(C−H); 1091 vs; 1063 vs, ν(S=O); 414 s, ν(Ru−S).

Physical Measurements. Elemental analyses were carried out at the Microanalytical Service of the Institute of Physical Chemistry of the University of Vienna. Infrared spectra were recorded on a Perkin-Elmer FTIR 2000 IR spectrometer in KBr pellets (4000−400 cm^{-1}). UV−vis spectra were recorded on a Perkin-Elmer Lambda 20 UV/vis spectrometer using samples dissolved in chloroform or methanol. Electrospray ionization mass spectrometry was carried out with a Bruker Esquire 3000 instrument (Bruker Daltonic, Bremen, Germany). The given *m*/*z* values, originating from the most intense isotopes, were obtained by the mass linearization procedure. Expected and experimental isotope distributions were compared. Cyclic voltammograms were measured in a two-compartment three-electrode cell using a 0.8-mm-diameter platinum-disk working electrode, connected to a silver-wire pseudoreference electrode and a platinum auxiliary electrode. Measurements were performed at room temperature using an Jaissle 1001-T NC potentiostat and a digital data recording system (SCADA). Deaeration of solutions was accomplished by passing a stream of high-purity argon through the solution for 10 min prior to the measurements and then maintaining a blanket atmosphere of argon over the solution during the measurements. The potentials were measured in 0.15 M [*n*-Bu$_4$N][BF$_4$]/DMF or DMSO, using the $[Fe(\eta^5\text{-}C_5H_5)_2]^{0/+}$ ($E_{1/2}^{ox}$ = 0.72 or 0.68 V vs NHE in DMF or DMSO, respectively)[19,20] and the $[Ru^{III/IV}Cl_4(Hind)_2]^{-/0}$ ($E_{1/2}^{ox}$ = 1.27 V [21] vs NHE in DMF or DMSO) couples as internal standards, and are quoted relative to NHE. Kinetic measurements were undertaken in 4 mM solutions of the complexes in DMF at 298 K using a LAUDA RC6 thermostat. The theoretical values of rate constants were obtained by simulation with software package ESP2.4.[22]

Crystallographic Structure Determination. X-ray diffraction measurements were performed on a Nonius Kappa CCD diffractometer at 120 K. Single crystals were positioned at 30 mm from the detector, and 379, 330, 220, and 484 frames were measured, each for 25, 120, 150, and 15 s over a 2, 2, 2, and 1.5° scan for **1a**,**b**, **2**, and **5**, correspondingly. The data were processed using Denzo-SMN software. Crystal data, data collection parameters, and

(19) Barette, W. C., Jr.; Johnson, H. W., Jr.; Sawyer, D. T. *Anal. Chem.* **1984**, *56*, 1890−1898.
(20) Guedes da Silva, M. F. C.; Pombeiro, A. J. L.; Geremia, S.; Zangrando, E.; Calligaris, M.; Zinchenko, A. V.; Kukushkin, V. Yu. *J. Chem. Soc., Dalton Trans*. **2000**, 1363−1371.
(21) Reisner, E.; Arion, V. B.; Guedes da Silva, M. F. C.; Lichtenecker, R.; Eichinger, A.; Keppler, B. K.; Kukushkin, V. Yu.; Pombeiro, A. J. L. *Inorg. Chem.* **2004**, *43*, 7083−7093.
(22) Nervi, C. (nervi@lem.ch.unito.it). *Electrochemical Simulation Package (ESP*, version 2.4); Dipartimento di Chimica, IFM: Torino, Italy, 1994/98.

structure refinement details for **1a**,**b**, **2**, and **5** are given in Table 1. The structures were solved by direct methods and refined by full-matrix least-squares techniques. Non-hydrogen atoms were refined with anisotropic displacement parameters. H atoms were located on difference Fourier maps and isotropically refined. Computer programs: structure solution, SHELXS-97;[23] refinement, SHELXL-97;[24] molecular diagrams, ORTEP;[25] scattering factors.[26]

Results and Discussion

Synthesis and Characterization of Complexes. The tetramethylammonium salt of *trans*-tetrachlorobis(indazole)-ruthenate(III) was used as starting material to avoid the concurrent Anderson's rearrangement reaction,[8,27] which implies the migration of the proton from the indazolium cation of KP1019 to one of the coordinated chloro ligands and release of HCl with subsequent occupation of the resulting vacancy by the indazole molecule. Reaction of $[Me_4N][trans\text{-}RuCl_4(Hind)_2]$ [λ_{max} (ϵ_M) = 296 (21250), 376 (5270), and 438 (680)] with 9-methyladenine in 1:2 molar ratio in ethanol at reflux for 1 h resulted in a raw material, which after purification by column chromatography on silica yielded 15% of a brown product *mer*,*trans*-$[Ru^{III}Cl_3(Hind)_2(made)]$, **1**, with absorbance features at λ_{max} (ϵ_M) = 380 (3300) and 428 (2030). X-ray diffraction quality rectangular plates of **1**·$1.1H_2O$·$0.9CH_3OH$, **1a**, and needles of **1**·CH_2Cl_2·CH_3OH, **1b**, were grown by slow diffusion of hexane in a dichloromethane solution of **1**, containing a few drops of methanol. $[Me_4N][trans\text{-}RuCl_4(Hind)_2]$ reacted with a large excess of dimethyl or diethyl sulfide at reflux for 1−2 h with reduction of ruthenium(III) to ruthenium(II) to give X-ray diffraction quality yellow-orange needles of *trans*,*trans*,*trans*-$[Ru^{II}Cl_2(Hind)_2(Me_2S)_2]$, **2** [$\lambda_{max}$ (ϵ_M) = 293 (6810) and 361 (12590)], and fine yellow-orange microcrystals of *trans*,*trans*,*trans*-$[Ru^{II}Cl_2(Hind)_2(Et_2S)_2]$, **3** [$\lambda_{max}$ (ϵ_M) = 297 (6750) and 369 (14300)], in 45 and 75% yield, correspondingly. Oxidation of **2** and **3** with hydrogen peroxide/12 M HCl in chloroform led to substitution of one of the two dialkyl sulfide ligands by a chloride ion and formation of brown products *mer*,*trans*-$[Ru^{III}Cl_3(Hind)_2(Me_2S)]$, **4**, with λ_{max} (ϵ_M) = 286 (17450), 366 (3800), and 444 (1850) and *mer*,*trans*-$[Ru^{III}Cl_3(Hind)_2(Et_2S)]$, **5**, with λ_{max} (ϵ_M) = 287 (23150), 384 (3620), and 446 (2760) in 20 and 76% yield, respectively. Single crystals of **5** suitable for X-ray diffraction analysis were grown by slow vapor diffusion of pentane into a chloroform solution of **5**. From a DMSO solution of **2** or **3** at room temperature via replacement of both R_2S ligands by DMSO molecules yellow microcrystalline plates of *trans*,*trans*,*trans*-$[Ru^{II}Cl_2(Hind)_2(DMSO)_2]$, **6**, have been isolated in 53% or 78% yield, respectively. Our attempts to prepare single crystals of **6** for an X-ray data set collection resulted in crystals of rather poor quality, which however permitted us to establish the configuration of the complex as a trans,trans,trans isomer. The positive ion ESI mass spectrum of **1** showed a 100% intense peak at *m*/*z* 557 due to $[Ru^{III}Cl_2(Hind)_2(made)]^+$ ion, while the negative ion ESI mass spectrum displayed a 100% intense peak at *m*/*z* 593 which was attributed to $[Ru^{III}Cl_3(Hind)_2(made) - H]^-$ and three other peaks at *m*/*z* 629, 480, and 326 with relative intensities 40, 65, and 25% due to $[Ru^{III}Cl_3(Hind)_2(made) + Cl]^-$, $[Ru^{III}Cl_4(Hind)_2]^-$, and $[Ru^{III}Cl_3(ind)]^-$ ions. Their isotopic patterns in the mass spectra agreed well with the calculated isotopic distribution. While the positive ion mass spectrum of **2** contained peaks at *m*/*z* 532 and 497, which were assigned to $[Ru^{III}Cl_2(Hind)_2(Me_2S)_2]^+$ and $[Ru^{II}Cl(Hind)_2(Me_2S)_2]^+$ ions, in the mass spectrum of **3** two peaks with *m*/*z* 498 and 408 with relative intensity 70 and 100% were observed, attributable to $[Ru^{III}Cl_2(Hind)_2(Et_2S)]^+$ and $[Ru^{III}Cl_2(Hind)_2]^+$. The mass spectrum of **4** showed three peaks at *m*/*z* 532, 470, and 408 with relative intensity 100, 30, and 30%, presumably due to $[Ru^{III}Cl_2(Hind)_2(Me_2S)_2]^+$, arising in the ion source of the mass spectrometer, $[Ru^{III}Cl_2(Hind)_2(Me_2S)]^+$, and $[Ru^{III}Cl_2(Hind)_2]^+$ ions. A single peak at *m*/*z* 498 due to $[Ru^{III}Cl_2(Hind)_2(Et_2S)]^+$ was observed in the mass spectrum of **5**.

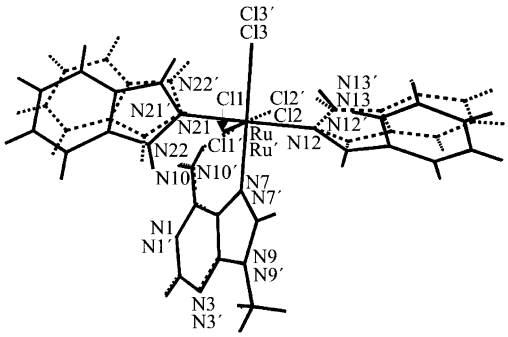

Figure 1. Superposition of the molecular structure of $[Ru^{III}Cl_3(Hind)_2(made)]$ in **1b** (solid line) on that in **1a** (dashed line), showing the difference in geometric parameters.

Crystal Structures. $[Ru^{III}Cl_3(Hind)_2(made)]$·$CH_2Cl_2$·$CH_3OH$ (**1a**) crystallized as rectangular plates in the triclinic space group $P\bar{1}$, while $[Ru^{III}Cl_3(Hind)_2(made)]$·$1.1H_2O$·$0.9CH_3OH$ (**1b**) crystallized as needles in the monoclinic space group $P2_1/n$. Both structures contain an essentially octahedral neutral complex $[Ru^{III}Cl_3(Hind)_2(made)]$ and solvent molecules, viz., CH_2Cl_2 and CH_3OH in **1a** and H_2O and CH_3OH in **1b**, which contribute to the stability of crystal lattices. The molecules of $[Ru^{III}Cl_3(Hind)_2(made)]$ adopt essentially the same geometry, differing mainly in the position of indazole rings (Figure 1). A part of the crystal structure of **1b** is shown in Figure 2, and selected bond distances and angles of the complex molecule in **1a**,**b** are quoted in Table 2. The ruthenium atom is bound to three chloride ions in a mer configuration, two indazole ligands in mutual trans positions, and one 9-methyladenine ligand completing the coordination sphere. The purine ligand is coordinated to ruthenium through nitrogen atom N7 in its amine form (Chart 1). The Ru−N7 bond length of 2.1039(17)

(23) Sheldrick, G. M. *SHELXS-97, Program for Crystal Structure Solution*; University Göttingen: Göttingen, Germany, 1997.
(24) Sheldrick, G. M. *SHELXL-97, Program for Crystal Structure Refinement*; University Göttingen: Göttingen, Germany, 1997.
(25) Johnson, C. K. *Report ORNL-5138*; OAK Ridge National Laboratory: Oak Ridge, TN, 1976.
(26) *International Tables for X-ray Crystallography*; Kluwer Academic Press: Dordrecht, The Netherlands, 1992; Vol. C, Tables 4.2.6.8 and 6.1.1.4.
(27) Kukushkin, Yu. N. In *Chemistry of Coordination Compounds*; Vysshaya shkola: Moscow, 1985; p 406.

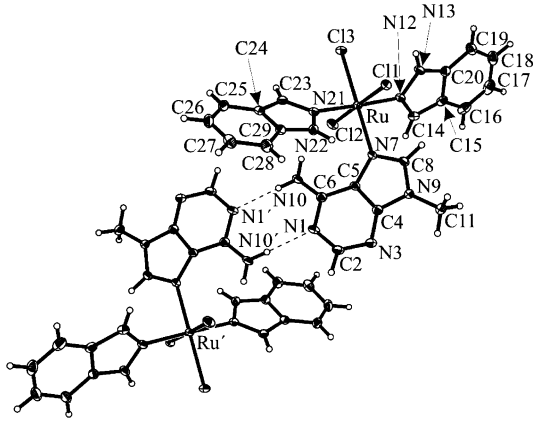

Figure 2. Part of the crystal structure of **1b** showing the coordinated 9-methyladenine pairing via intermolecular hydrogen-bonding interactions. Donor···acceptor (D···A) distances (Å) and donor-hydrogen···acceptor (D−H···A) angles (deg) of the intermolecular hydrogen bonds: N1···N10^{i} 2.986 Å, N1··H10^{i-N10i} 178.4°; atoms marked with i are at symmetry positions $-x + 1$, $-y$, $-z + 1$.

Table 2. Selected Bond Distances (Å) and Angles (deg) in **1a**,**b** and 9-Methyladenine

atom 1−atom 2	**1a**	**1b**	9-methyladenine
Ru−N7	2.1039(17)	2.101(2)	
Ru−N12	2.0748(19)	2.074(2)	
Ru−N21	2.069(2)	2.061(2)	
Ru−Cl1	2.3416(8)	2.3434(8)	
Ru−Cl2	2.3450(8)	2.3422(9)	
Ru−Cl3	2.3315(8)	2.3462(9)	
N1−C2	1.335(3)	1.342(4)	1.335(2)
C2−N3	1.335(3)	1.327(4)	1.326(2)
N3−C4	1.343(3)	1.344(4)	1.351(2)
C4−C5	1.388(3)	1.385(4)	1.380(2)
C5−C6	1.422(3)	1.421(4)	1.411(2)
C6−N1	1.358(3)	1.356(4)	1.357(2)
C6−N10	1.327(3)	1.331(4)	1.329(2)
C4−N9	1.370(3)	1.376(4)	1.370(2)
N9−C8	1.349(3)	1.347(4)	1.365(2)
C8−N7	1.320(3)	1.324(4)	1.311(2)
N7−C5	1.422(3)	1.405(4)	1.389(2)
N9−C11	1.463(3)	1.465(4)	1.453(3)

atom 1−atom 2−atom 3	**1a**	**1b**	9-methyladenine
C5−C6−N10	126.09(19)	126.3(3)	124.3(1)
C6−N1−C2	120.00(18)	119.3(3)	118.7(1)
N10−C6−N1	117.18(18)	116.8(3)	118.4(1)
C4−C5−N7	107.96(17)	108.6(2)	110.3(1)
C6−C5−N7	135.52(19)	135.0(3)	132.9(1)
N3−C4−N9	125.53(19)	125.3(3)	126.2(1)

Chart 1. Tautomeric Structures of 9-Methyladenine: Imine Form (Left); Amine Form (Middle); Zwitterionic Form (Right)

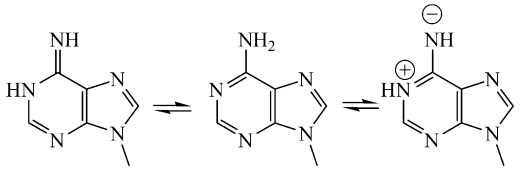

Å in **1a** and 2.101(2) Å in **1b** is significantly longer (>9σ)[28] than the Ru−N12 and Ru−N21 distances at 2.0748(19), 2.069(2) Å (**1a**) and 2.074(2), 2.061(2) Å (**1b**). The Ru−Cl distances are very similar in **1a**,**b** (Table 2) and compare well with those in [RuCl$_3$(Hind)$_3$] at 2.3335(15), 2.3449(16), and 2.3496(15) Å.[29] The angles at Ru atom do not deviate from 90 and 180° by more than 2.7 and 3.8° in **1a**,**b**, correspondingly. The C6−N10 bond length of 1.327(3) Å in **1a** and 1.331(4) Å in **1b** is significantly longer than the analogous bond at 1.293(3) Å in the metalated tautomeric imine form.[30] To analyze the influence of the 9-methyladenine coordination to the ruthenium(III) center, the bond lengths and angles of the coordinated purine ligand in **1a**,**b** have been compared with those of metal-free 9-methyladenine.[31] The corresponding bond lengths of the purine base moieties in **1a**,**b** are very similar (Table 2), and they do not significantly deviate from the values given for metal-free 9-methyladenine. The largest differences in geometric parameters are observed for N7−C5, N7−C8, and C8−N9 bond lengths and C4−C5−N7 and C6−C5−N7 bond angles, comprising the atoms which are in the close proximity to the ruthenium center. It should also be noted that the angle C6−N1−C2 in **1a**,**b** is at 120.00(18) and 119.3(3)°, respectively, what compares well with that in 9-methyladenine at 118.7(1)° but is significantly smaller than that in 9-methyladenine dihydrobromide at 124°,[32] in which the N1 and N7 sites are protonated.

The planar trans-arranged indazole ligands are almost perpendicular to each other in **1a**,**b**. The torsion angle $\Theta_{N13-N12\cdots N21-N22}$ is at −97.7 (**1a**) and −92.0° (**1b**). Both indazole ligands (coordinated via N12 and N21) are tilted relative to the mean plane through RuN21N12N7Cl3, the corresponding angles being at 57.3 and 44.4° (**1a**) and 47.6 and 149.9° (**1b**).

Like in Watson−Crick interactions in DNA, the amino group acts in both compounds **1a**,**b** as a hydrogen donor and N1 as hydrogen acceptor, which are involved in complex pairing through strong intermolecular hydrogen bonding as shown in Figure 2 for **1b**: N10···N1($-x + 2$, $-y + 2$, $-z + 1$) = 2.982 Å, ∠N10HN1 = 175.38 (**1a**); N10···N1($-x + 1$, $-y$, $-z + 1$) = 2.986 Å, ∠N10HN1 = 178.38° (**1b**). It is also worth mentioning the intramolecular N10H···Cl2 hydrogen bond, which resulted in formation of a six-membered pseudometallocycle in the coordination sphere of ruthenium. The geometric parameters of this bond, N10···Cl2 = 3.160 Å, NH···Cl2 = 2.412 Å, and ∠N10HCl2 = 145.7° (**1b**), are typical for such kind of H-bond, determining to a large extent the arrangement of ligands around central metal atom.

From the supramolecular point of view the crystal structure of **1b** can be described as consisting of two-dimensional (2D) sheets (Figure S1, Supporting Information) separated by water and methanol molecules and oriented parallel to the crystallographic plane *ab*. Formation of these sheets is due to intermolecular hydrogen-bonding interactions NH···Cl and

(28) σ is defined as $(\sigma_1^2 + \sigma_2^2)^{1/2}$ with σ_1 and σ_2 being the standard uncertaintes for the bond lengths being compared.

(29) Pieper, T.; Sommer, M.; Galanski, M.; Keppler, B. K.; Giester, G. *Z. Anorg. Allg. Chem.* **2001**, *627*, 261−265.
(30) Velders, A. H.; van der Geest, B.; Kooijman, H.; Spek, A. L.; Haasnoot, J. G.; Reedijk, J. *Eur. J. Inorg. Chem.* **2001**, 369−372.
(31) (a) Stewart, R. F.; Jensen, L. H. *J. Chem. Phys.* **1964**, *40*, 2071−2075. (b) Kistenmacher, T. J.; Rossi, M. *Acta Crystallogr.* **1977**, *B33*, 253−257. (c) McMullan, R. K.; Benci, P.; Craven, B. M. *Acta Crystallogr.* **1980**, *B36*, 1424−1430.
(32) Bryan, R. F.; Tomita, K. *Acta Crystallogr.* **1962**, *15*, 1179−1182.

Table 3. Selected Bond Distances (Å) and Angles (deg) in **2**

atom 1−atom 2	distance	atom 1−atom 2	distance
Ru−S1	2.3674(10)	S1−C8	1.763(5)
Ru−N1	2.076(3)	S1−C9	1.773(4)
Ru−Cl1	2.4297(9)		

atom 1−atom 2−atom 3	angle	atom 1−atom 2−atom 3	angle
S1−Ru−N1	90.78(8)	C8−S1−C9	98.2(3)
S1−Ru−Cl1	87.95(4)	N1−Ru−S1*	89.22(8)
Cl1−Ru−S1*	92.05(4)	N1−Ru−N1*	180.0
S1−Ru−S1*	180.0	Cl1−Ru−Cl1*	180.0

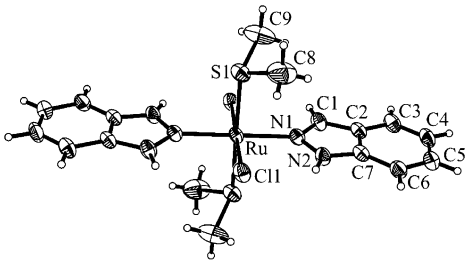

Figure 3. View of the molecule of **2**, showing the atom-labeling scheme. Displacement ellipsoids are drawn at the 50% probability level.

CH···Cl, along with $\pi-\pi$ stacking interactions. By consideration of these interactions, the building of centrosymmetric dimers (Figure S2) held together by four short contacts NH···Cl with N13H···Cl1′($-x$, $-1-y$, $-1-z$) = 2.824 Å, N13H···Cl3 = 2.774 Å, ∠N13HCl1 = −130°, and ∠N13HCl3 = −134° can be observed. Further extension of this dimeric fragment to a 2D sheet occurs via H bonding with participation of the NH_2 group and CH···Cl contacts (C26H···Cl′(x, $-y-1$, $-z$) = 2.875 Å, ∠C26HCl′ = 132.2°). The interplanar separation between the two 9-methyladenine ligands with antiparallel orientation is at 3.402 Å, indicating the involvement of $\pi-\pi$ stacking interactions in the formation of the 2D network.

The dihedral angle between the mean plane of the purine ligand and that through RuCl1Cl2Cl3N7 is ca. 49.5° in **1a** and 50.3° in **1b** and seems to be controlled by intramolecular H bond N10H···Cl2 and the just mentioned $\pi-\pi$ stacking interactions. Another orientation of adenine ligands is precluded by steric repulsions with Cl2 and one of the indazole ligands (Figure 2).

The complex $[Ru^{II}Cl_2(Hind)_2(Me_2S)_2]$ (**2**) crystallizes in the centrosymmetric *C*2/*c* space group with Ru atom lying in the center of symmetry (0, 0, $^1/_2$) and the asymmetric unit consisting of half the molecule. The complex has essentially octahedral coordination around the ruthenium atom. Bond angles with Ru as vertex (Table 3) are all within 2.1° of the values for an ideal octahedron. The two sulfides, the two chlorides, and the two indazole ligands are all correspondingly trans to each other (Figure 3). The complex $[Ru^{III}Cl_3(Hind)_2(Et_2S)]$ (**5**) crystallized in a monoclinic space group $P2_1/c$ with two independent molecules/asymmetric unit. Three chloride atoms and the sulfur atom of the Et_2S ligand in the equatorial plane along with two axial indazole ligands form a distorted octahedron about ruthenium atom. The Et_2S ligand showed a two-site positional disorder in both independent molecules, the extent of which was larger in the second molecule. The structure of the first independent

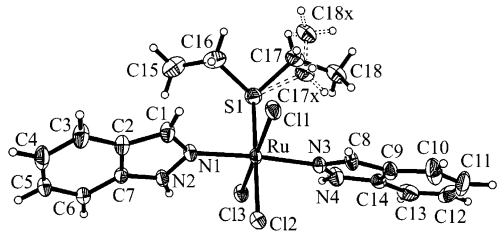

Figure 4. View of a molecule of **5**, showing the atom-labeling scheme. Displacement ellipsoids are drawn at the 50% probability level.

Table 4. Selected Bond Distances (Å) and Angles (deg) in One of the Two Independent Molecules of **5**

atom 1−atom 2	distance	atom 1−atom 2	distance
Ru1−S1	2.3883(11)	Ru1−Cl1	2.3471(10)
Ru1−N1	2.080(3)	Ru1−Cl2	2.3598(10)
Ru1−N3	2.068(3)	Ru1−Cl3	2.3437(10)

atom 1−atom 2−atom 3	angle	atom 1−atom 2−atom 3	angle
N1−Ru1−N3	174.37(14)	Cl3−Ru1−Cl2	93.82(4)
Cl3−Ru1−S1	86.70(4)	Cl1−Ru1−Cl2	90.87(4)
Cl1−Ru1−S1	88.62(4)	N1−Ru1−S1	93.39(10)

molecule is shown in Figure 4, and selected bond lengths and angles are in Table 4.

$Ru^{II}-S$ bond distances have been reported[33,34] to span a wide range from 2.188(3) Å in $[(NH_3)_5Ru^{II}(DMSO)](PF_6)_2$[35] to 2.450(3) Å for one of the *cis*-thiobenzoato ligands in $Ru^{II}(phen)(PMe_2Ph)_2(PhC(O)S)_2$.[36] This variation in distance has been attributed in part to varying amounts of π-backbonding arising from overlap of filled Ru d(π) orbitals with vacant antibonding orbitals of π-acceptor ligands such as thioethers or DMSO.[34] In contrast to the Ru−Cl distances, which are longer for the Ru(II) species (e.g., Ru−Cl1 at 2.4297(9) Å in **2** compared to Ru1−Cl1 at 2.3470(10), Ru1−Cl2 at 2.3599(10), and Ru1−Cl3 at 2.3441(10) Å in $[Ru^{III}Cl_3(Hind)_2(Et_2S)]$ (**5**)), the $Ru^{II}-S1$ distance (Table 3) is 0.021 Å (or 14σ) shorter than that in the Ru^{III} species for the independent molecule with no disorder affecting this bond at 2.3884(11) Å, implying some contribution of backbonding. The Ru−N1 distance at 2.076(3) Å is comparable with the two Ru−N bond lengths in $[Ru^{III}Cl_3(Hind)_2(Et_2S)]$ (**5**) at 2.078(3) and 2.065(3) Å.

The thioether ligands in **2** and **5** are linked to Ru with pyramidal coordination about S, as has been observed for other Ru−thioether complexes.[33,37] In contrast to $[(NH_3)_5Ru(EtSMe)]^{2+}$,[34] where the S atom lies below the equatorial plane defined by Ru and three nitrogen atoms, the S atoms in **2** lie in the plane defined by Ru, Cl1, and S1 (Figure 3), while the carbon atoms C8 and C9 and centrosymmetrically related C8* and C9* bonded to S1 and S1*, respectively, lie above and correspondingly below this plane. The Ru−S1−Y angle at 124.4°, where Y is the midpoint of the

(33) James, B. R.; Pacheco, A.; Rettig, S. J.; Ibers, J. A. *Inorg. Chem.* **1988**, *27*, 2414−2421.
(34) Krogh-Jespersen, K.; Zhang, X.; Ding, Y.; Westbrook, J. D.; Potenza, J. A.; Schugar, H. J. *J. Am. Chem. Soc.* **1992**, *114*, 4345−4353.
(35) March, F. C.; Ferguson, G. *Can. J. Chem.* **1971**, *49*, 3590−3595.
(36) Gould, R. O.; Stephenson, T. A.; Thomson, M. A. *J. Chem. Soc., Dalton Trans.* **1980**, 804−809.
(37) Krogh-Jespersen, K.; Zhang, X.; Westbrook, J. D.; Fikar, R.; Nayak, K.; Kwik, W.-L.; Potenza, J. A.; Schugar, H. J. *J. Am. Chem. Soc.* **1989**, *111*, 4082−4091.

C8···C9 vector, gives an estimate of the dihedral angle between the C8−S1−C9 plane and the plane through Ru1, S1, and Cl1. The S−C distances and C−S−C angle are slightly smaller than those reported for nonbonded dimethyl thioether [1.807(2) Å and 99.05(4)°].[38]

While the S atom in **5** also lies in the equatorial plane defined by Ru and three Cl atoms, the carbon atoms C15, C16 and C17, C18 (along with C17x and C18x) are placed above and correspondingly below this plane and not at the same side of the equatorial plane as in **2**. Steric interactions between the alkyl groups of the coordinated Et_2S ligand with axial indazole ligands result in slight nonlinearity of the N1−Ru−N3 group, the angle being at 174.37(14)°. The distances within indazole ligands in **5** are normal.[18]

Coordination Mode of 9-Methyladenine. The coordination chemistry of 9-substituted adenine derivatives shows interesting features mainly because of the diverse modes of binding to metal ions and tautomerism. A comprehensive discussion of this topic is available.[39] Briefly, of the five nucleoside bases cytosine, thymine, uracyl, guanine, and adenine as constituents of DNA and RNA, the adenine moiety displays the most flexible binding-site behavior toward metal ions.[40] Coordination of 9-substituted adenine via the ring nitrogen atoms is governed first of all by their basicity, which decreases in the order N1 > N7 > N3. In some cases, metal ions can also bind to the exocyclic amino group with concomitant loss of a proton or its migration to the neighboring ring nitrogen atom N1 and stabilization of the rare imine tautomer (Chart 1).[41] In addition, the mode of binding of 9-substituted adenine derivatives in aqueous solution also depends on pH, the metal, and the presence of other ligands. Along with the monodentate mode of binding, bridging and/or chelate interactions involving almost all possible combinations of exocyclic and endocyclic nitrogen atoms and even the C8 of imidazole ring have been established by X-ray diffraction methods.[42] Surprisingly, no crystallographic evidence for monodentate coordination mode of 9-alkyladenine to ruthenium has been documented so far. There are known however a few examples of bridging and/or chelate interactions involving the exocyclic nitrogen atom N10, the ring nitrogen atoms, and the C8 of the imidazole ring. The trimeric complex [{Ru(etad-H)(η^6-*p*-cymene)}$_3$](CF$_3$SO$_3$)$_3$ exhibits the μ-1κN^1:2κ^2N^6,N^7 coordination mode.[43]

Chart 2. Sterically Unfavorable (a) and Observed (b) Orientations of SC_2 Planes of Thioether to the Median RuS_2Cl_2 Plane

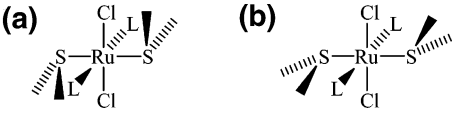

Ruthenium binding to C8 of adenine, supported by a chelating residue at the 9-position, has also been reported.[44] Binding to the exocyclic amino group which is accompanied by deprotonation and migration of the amino proton to the ring nitrogen atom N1, stabilizing the rare imine tautomer, has also been observed for ruthenium.[30]

In complex **1**, which crystallized in the triclinic space group $P\bar{1}$ as **1**·CH_2Cl_2·CH_3OH and in the monoclinic space group $P2_1/n$ as **1**·1.1H_2O·0.9CH_3OH, the coordination to ruthenium via N7 has been found, the atom which, in opinion of some authors,[30] is not necessarily the most likely binding site of aminopurines to ruthenium. This is the first crystallographic evidence for monodentate coordination of 9-substituted adenine to ruthenium. Interestingly, binding did not occur via the more basic ring nitrogen N1. Instead N1 and N10 are involved in intermolecular interactions leading to self-pairing of 9-methyladenine molecules. These interactions probably determine the metal-binding site. In this context, it is noteworthy to mention the macrocyclic organopalladium complexes [(thiacyclophane)Pd(adenine)]$^+$,[45] where the atypical metal−N3 monodentate binding is directed by the formation of hydrogen bonds between the exocyclic amino group and ether oxygens of the thiacyclophane ligand.

Binding of Thioethers. The highest occupied molecular orbital in a thioether is an out-of-plane lone pair concentrated (>90%) on the S atom, S(π), that is perpendicular to the SC_2 plane. This can serve as a good electron donor. The next two occupied orbitals, the symmetric and antisymmetric combinations of S−C bond orbitals, lie ca. 3−4.5 eV lower in energy according to both computational calculations[34] and experimental estimate (PES)[46,47] and are spatially and energetically far from optimal to be involved in metal−ligand bonding. The second lone pair was found to be mainly of 3s character having even lower energy than the S−C bond orbitals.[37] On the Ru atom, the main acceptor orbital for thioether electron density is the empty $d_{x^2-y^2}$ orbital of the e_g* set of 4d orbitals. Maximal S(π)−d(σ*) overlap would require a fully perpendicular orientation of the SC_2 plane of thioether to the equatorial RuS_2Cl_2 plane. However, this orientation is sterically most unfavorable (Chart 2a). Therefore, the Ru−S1−Y (Y = midpoint of the C···C vector) angle resulted as a compromise between the bonding requirements of the thioether ligand and steric repulsions between the indazoles and thioethers (Chart 2b).[37]

(38) Iijima, T.; Tsuchiya, S.; Kimura, M. *Bull. Chem. Soc. Jpn.* **1977**, *50*, 2564−2567.
(39) (a) Lippert, B. *Coord. Chem. Rev.* **2000**, *200*−*202*, 487−516. (b) Salam, M. A.; Aoki, K. *Inorg. Chim. Acta* **2000**, *311*, 15−24.
(40) Arpalahti, J.; Klika, K. D.; Molander, S. *Eur. J. Inorg. Chem.* **2000**, 1007−1013.
(41) (a) Kuo, L. Y.; Kanatzidis, M. G.; Sabat, M.; Tipton, A. L.; Marks, T. J. *J. Am. Chem. Soc.* **1991**, *113*, 9027−9045. (b) Zamora, F.; Kunsman, M.; Sabat, M.; Lippert, B. *Inorg. Chem.* **1997**, *36*, 1583−1587. (c) Clarke, M. J. *J. Am. Chem. Soc.* **1978**, *100*, 5068−5075. (d) Arpalahti, J.; Klika, K. D. *Eur. J. Inorg. Chem.* **1999**, 1199−1201. (e) Viljanen, J.; Klika, K. D.; Sillampää, R.; Arpalahti, J. *Inorg. Chem.* **1999**, *38*, 4924−4925.
(42) (a) Trovó, G.; Bandoli, G.; Nicolini, M.; Longato, B. *Inorg. Chim. Acta* **1993**, *211*, 95−99. (b) Olivier, M. J.; Beauchamp, A. L. *Acta Crystallogr.* **1982**, *B38*, 2159−2162. (c) Prizant, L.; Olivier, M. J.; Rivest, R.; Beauchamp, A. L. *J. Am. Chem. Soc.* **1979**, *101*, 2765−2767.
(43) Korn, S.; Sheldrick, W. S. *Inorg. Chim. Acta* **1997**, *254*, 85−91.
(44) Price, C.; Elsegood, M. R. J.; Clegg, W.; Rees, N. H.; Houlton, A. *Angew. Chem., Int. Ed. Engl.* **1997**, *36*, 1762−1764.
(45) Kickham, J. E.; Loeb, S. J.; Murphy, S. L. *Chem.—Eur. J.* **1997**, *3*, 1203−1213.
(46) Frost, D. C.; Herring, F. G.; Katrib, A.; McDowell, C. A.; McLean, R. A. N. *J. Phys. Chem.* **1972**, *76*, 1030−1034.
(47) Cradock, S.; Whiteford, R. A. *J. Chem. Soc., Faraday Trans. 2* **1972**, *68*, 281−288.

Table 5. Cyclic Voltammeric Data for **1**−**5** and Estimated Redox Potential Values

	exptl[a]		calcd[b]	
complex	$E_{1/2}$/I$^{red/ox}$	$E_{1/2}$/a[c]	$E_{1/2}$/I	$E_{1/2}$/a
[Ru^{III}Cl$_3$(Hind)$_2$(made)] (**1**)	0.02 (0.03)	0.36 (0.93)		
[Ru^{II}Cl$_2$(Hind)$_2$(Me$_2$S)$_2$] (**2**)	0.72 (0.68)	0.51 (1.11)	0.68	0.42 (0.93)
[Ru^{II}Cl$_2$(Hind)$_2$(Et$_2$S)$_2$] (**3**)	0.73 (0.69)	0.53 (1.10)	0.76	0.46 (0.97)
[Ru^{III}Cl$_3$(Hind)$_2$(Me$_2$S)] (**4**)	0.16 (0.18)	0.51 (0.95)	0.15	0.42 (0.93)
[Ru^{III}Cl$_3$(Hind)$_2$(Et$_2$S)] (**5**)	0.17 (0.17)	0.53 (0.94)	0.19	0.46 (0.97)

[a] Potentials in V ± 0.02 vs NHE measured at a scan rate of 0.305 V s^{-1}, in 0.15 M [*n*-Bu$_4$N][BF$_4$]/DMF (or DMSO, in parentheses). [b] Potentials in V vs NHE estimated from eq 1 with S_M and I_M values of 0.97 and 0.04, respectively, and known E_L for the ligands (see text). Values in parentheses refer to the DMSO derivative. [c] Oxidation waves detected upon scan reversal after the formation of wave I^{red} (**1**, **4**, **5**) or shortly after dissolution (**2**, **3**) (see text).

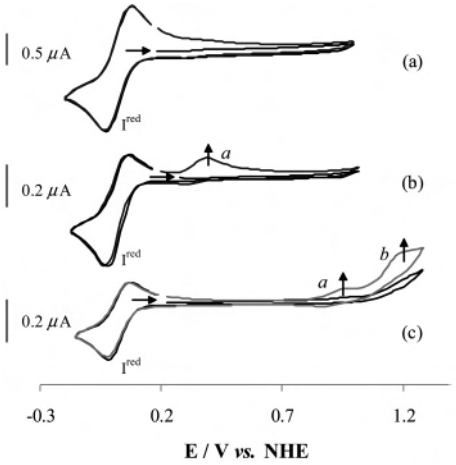

Figure 5. Cyclic voltammograms of 2 mM [RuCl$_3$(Hind)$_2$(made)] solutions in DMF (a, b) or DMSO (c) with 0.15 M [*n*-Bu$_4$N][BF$_4$], at a platinum-disk working electrode and at a scan rate of 0.305 V s^{-1} in (a) or 0.03 V s^{-1} in (b) and (c). The black line indicates the first and the gray line the second scan.

Electrochemical Studies. The cyclic voltammograms (CVs) of 0.15 M [*n*-Bu$_4$N][BF$_4$]/DMF or DMSO solutions of [Ru^{III}Cl$_3$(Hind)$_2$(made)] (**1**), [Ru^{III}Cl$_3$(Hind)$_2$(Me$_2$S)] (**4**), and [Ru^{III}Cl$_3$(Hind)$_2$(Et$_2$S)] (**5**) at a platinum disk working electrode at a scan rate of 0.305 V s^{-1} display one quasi-reversible one-electron reduction wave, I^{red}, which is assigned to the Ru^{III} → Ru^{II} process at 0.02−0.03 V (Table 5, Figure 5) and at 0.16−0.18 V vs NHE (Table 5, Figure 6a,c) for **1** and **4** and **5**, correspondingly. Upon scan reversal following the formation of wave I^{red}, one oxidation wave, wave a, is detected at 0.36 V in DMF and 0.93 V in DMSO (**1**) and at 0.51−0.53 V in DMF and 0.94−0.95 V in DMSO (**4**, **5**), being due to the oxidation of products formed in the cathodic processes. The current function ($i_p v^{-1/2} c^{-1}$, where i_p is the peak current, v the scan rate, and c the concentration) of the genuine oxidation wave, I^{ox}, which is maximum at high scan rates, decreases with the decrease of the scan rate with concomitant increase of the current function of the oxidation wave a (Figure 5a,b) that indicates the cathodic formation of a thermodynamic product derived from the original complex. The visible spectra of **1** in DMF or DMSO do not show any major change when monitored over 10 h (Figure S3).

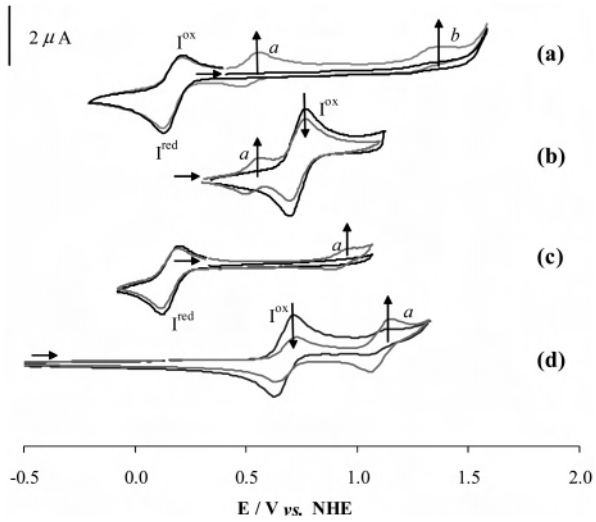

Figure 6. Cyclic voltammograms of 2 mM [RuCl$_3$(Hind)$_2$(Et$_2$S)] (**5**) (a, c) and [Ru^{II}Cl$_2$(Hind)$_2$(Et$_2$S)$_2$] (**3**) (b, d) solutions in DMF (a, b) or DMSO (c, d) with 0.15 M [*n*-Bu$_4$N][BF$_4$], at a platinum-disk working electrode and at a scan rate of 0.305 V s^{-1}. The black line indicates the first and the gray the second scan cycle upon reduction (a and c). The CV curve in black was recorded immediately (b) or 0.05 h (d) and in the case of the gray line 0.1 h (b) and 0.5 h (d) after dissolution of the complex.

The cyclic voltammograms of 0.15 M [*n*-Bu$_4$N][BF$_4$]/DMF or DMSO solutions of the complexes [Ru^{II}Cl$_2$(Hind)$_2$(Me$_2$S)$_2$] (**2**) and [Ru^{II}Cl$_2$(Hind)$_2$(Et$_2$S)$_2$] (**3**) at a platinum disk working electrode and at a scan rate of 0.305 V s^{-1} display (Figure 6b,d) one one-electron oxidation wave, I^{ox}, which is assigned to the Ru^{II} → Ru^{III} process at 0.68−0.73 V vs NHE (Table 5). Running a CV immediately upon dissolution of the complexes did not show any further waves, but after a few minutes a new wave, wave a, arises depending on the solvent at 0.51−0.53 V in DMF or 1.10−1.11 V in DMSO concomitant with a time-dependent decrease of the current ratio $^{I}i_p^{ox}/^{I}i_p^{red}$ of the genuine Ru^{III}/Ru^{II} redox couple. This behavior is in accord with the time-dependent spectrophotometric profiles for **2** and **3** in DMF or DMSO. In particular, the absorbance band of the complex **3** in DMF at 371 nm (band I) disappears with the concomitant increase of the absorption (band a) at 296 nm (Figure S4). A clear isosbestic point is observed at 331 nm, indicating an equilibrium between two species.

The $E_{1/2}$ values for the Ru^{III}/Ru^{II} redox couple in complexes **2**, **3** and **4**, **5** fit well with those expected on the basis of the general eq 1, by using the known values of S_M and I_M (0.97 and 0.04, respectively)[48] and the E_L values for the various ligands [E_L(Hind) = 0.26,[21] E_L(Cl$^-$) = −0.24,[48] E_L(Me$_2$S) = 0.31,[48] E_L(Et$_2$S) = 0.35[48] (Table 5)]. Moreover, considering the experimental values of the redox potentials of **1** in DMF and DMSO, the yet unknown E_L ligand parameter for 9-methyladenine is estimated as an average of two values (one for DMF and another for DMSO) at 0.18 V vs NHE. This value is in the range of unsaturated amines of stronger π-acid character than pyridines, bipyridines, and azoles, e.g., E_L(imidazole) = 0.12.[48] The E_L value is, as expected, higher than that for the imidazole because of a decrease of the net

(48) Lever, A. B. P. *Inorg. Chem.* **1990**, *29*, 1271−1285.

Scheme 2. Proposed Cathodic Processes of Complexes **4** and **5** with S = DMF or DMSO

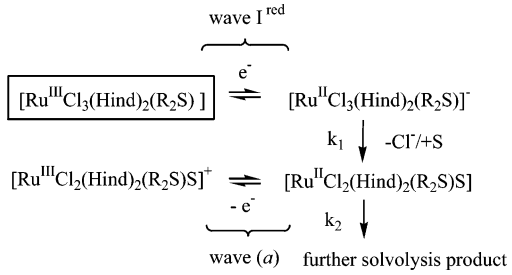

electron donor character (increase of E_L) due to the annelated pyrimidine ring.

$$E = S_M \sum E_L + I_M \quad (1)$$

The cathodically induced metal dechlorination on solvolysis for this type of compounds is a well-documented type of reaction for Ru(III) complexes[21] and results in solvent dependent redox potentials of wave a. Thus, the formation of [Ru^{II}Cl$_2$(Hind)$_2$(R$_2$S)S], where S is the solvent molecule, is suggested, which agrees rather well with Lever's approach [E_L(DMSO) = 0.57,[20] E_L(DMF) = 0.03[49] (Table 5)]. Oxidation of the replaced chloride is observed at $E_p = 1.20-1.25$ V in DMSO or 1.30−1.35 V in DMF upon reduction, labeled as wave b (Figures 5c and 6a), also observed for [Me$_4$N]Cl under the same experimental conditions and found to be consistent with reported observations.[21,50,51]

Interestingly, the redox potentials in DMF of wave a formed upon solvolysis of **2** and **3** are identical with wave a formed upon reduction in **4** and **5**. This indicates the formation of the same species, as shown in eq 2, viz., [RuCl$_2$(R$_2$S)(Hind)$_2$S], where S is the solvent molecule. In DMSO the redox potentials of wave a are similar (ΔE = 0.16 V) but not identical, which may be explained by formation of different geometric isomers and/or the poor behavior of the DMSO ligand that yields a variation of E_L spanning a range of ca. $\Delta E_L = 0.17$ V.[48,20] Replacement of thioether ligands by solvent molecules in **2** and **3** is further supported by the disappearance of wave I^{ox} and of wave a in DMSO after ca. 3 h, whereupon a yellow powder started to precipitate, which was isolated and shown to be *trans*,*trans*,*trans*-[RuCl$_2$(Hind)$_2$(DMSO)$_2$]. The same product was obtained in the absence of current after dissolution of **2** or **3** in DMSO (see Experimental Section).

$$[Ru^{III}Cl_3(Hind)_2(R_2S)] \xrightarrow[+S]{+e^-,\,-Cl^-} [Ru^{II}Cl_2(Hind)_2(R_2S)S] \xleftarrow[+S]{-R_2S} [Ru^{II}Cl_2(Hind)_2(R_2S)_2] \quad (2)$$

The mechanism depicted in Scheme 2 was investigated in detail by digital simulation of the cyclic voltammograms in the range of scan rates 0.002−10 V s^{-1} for complexes **4** and **5**. A good fit was obtained (Figure S5) for the degree of reversibility of the cathodic wave I^{red}, i.e., $^{I}i_p^{ox}/^{I}i_p^{red}$, and the extent of formation of the chloride displacement product, i.e., the normalized peak current of wave a, $^{a}i_p^{ox}/^{I}i_p^{red}$ (ρ), as a function of scan rate. Cyclic voltammograms at a scan rate higher than 5 V s^{-1} reveal a $^{I}i_p^{ox}/^{I}i_p^{red}$ ratio equal to 1. Upon decrease of the scan rate, there occurs an increasing conversion of original complex into the solvolysis products. The optimized value of the homogeneous rate constant k_1 for the first replacement of chloride by DMF is 0.9 ± 0.1 s^{-1} for both **4** and **5**. The reaction obeys a first-order rate law, i.e., is independent from the complex concentration. The homogeneous rate constant k_2 was determined to be 0.2 ± 0.1 M^{1-n}·s^{-1} with $n > 1$ for 4 mM solutions of complexes **4** and **5** and is concentration dependent indicating higher order rate law. As expected, no significant difference in the rate of solvolysis upon reduction could be observed between **4** and **5**.

Insight into Biological Action. The mode of action of ruthenium-based antitumor drugs is believed to differ from that of platinum in particular due to (i) the octahedral geometry of the former compared to the square-planar configuration of the latter and (ii) the facility of electron transfer for the Ru^{III}/Ru^{II} compared to the Pt^{IV}/Pt^{II} redox couple. There is now general agreement that the cytotoxicity of cisplatin, *cis*-[PtCl$_2$(NH$_3$)$_2$], originates from an intracellular hydrolysis of the chloro ligands and preferred binding of the activated aqua species to the target DNA via the N7 binding sites of the purine bases, guanine (G) and adenine (A), and the formation of 1,2-intrastrand d(GpG) (47−50%) and d(ApG) (23−28%) cross-links as the major adducts.[2a,52]

In view of the kinetic inertness of Ru^{III}−Cl bonds,[51,53,54] the occurrence of ruthenium−ligand exchange reactions resulting in the formation of **1**−**5** is rather intriguing. Although reduction facilitates Ru−Cl bond cleavage,[21] the activation is probably achieved by partial hydrolysis of *trans*-[RuCl$_4$(Hind)$_2$]$^-$ with formation of the more labile [RuCl$_3$(H$_2$O)(Hind)$_2$] complex and possibly the *trans*,*trans*,*trans*-[RuCl$_2$(H$_2$O)$_2$(Hind)$_2$]$^+$ complex. It should, however, be noted that bis-adduct formation for 9-methyladenine has not been observed in this study. Instead a favored monofunctional binding of one purine base via N7 to *trans*-[RuCl$_4$(Hind)$_2$]$^-$ occurred.

Gluthathione (GSH), a cysteine-containing tripeptide that is the most common cellular nonprotein thiol,[55] is readily oxidized to the disulfide at $E^{\circ\prime} = -0.25$ V vs NHE[56] {$E_{1/2}$ for *trans*-[RuCl$_4$(Hind)$_2$]$^-$ = 0.03 V[21]} and appears to be involved in the reduction of some Pt(IV) and Ru(III) complexes to the active Pt(II) and Ru(II) species.[15] In

(49) http://www.chem.yorku.ca/profs/lever (homepage of A. B. P. Lever).
(50) Arion, V. B.; Reisner, E.; Fremuth, M.; Jakupec, M. A.; Keppler, B. K.; Kukushkin, V. Yu.; Pombeiro, A. J. L. *Inorg. Chem.* **2003**, *42*, 6024−6031.
(51) Serli, B.; Zangrando, E.; Iengo, E.; Mestroni, G.; Yellowlees, L.; Alessio, E. *Inorg. Chem.* **2002**, *41*, 4033−4043.
(52) (a) Jamieson, E. R.; Lippard, S. J. *Chem. Rev.* **1999**, *99*, 2467−2498. (b) Fichtinger-Schepman, A. M. J.; van der Veer, J. L.; den Hartog, J. H. J.; Lohman, P. H. M.; Reedijk, J. *Biochemistry* **1985**, *24*, 707−713.
(53) Zanella, A. W.; Ford, P. C. *Inorg. Chem.* **1975**, *14*, 42−47.
(54) Coleman, G. N.; Gesler, J. W.; Shirley, F. A.; Kuempel, J. R. *Inorg. Chem.* **1973**, *12*, 1036−1038.
(55) Corazza, A.; Harvey, I.; Sadler, P. J. *Eur. J. Biochem.* **1996**, *236*, 697−705.
(56) Millis, K. K.; Weaver, K. H.; Rabenstein, D. L. *J. Org. Chem.* **1993**, *58*, 4144−4146.

addition, binding of GSH to ruthenium was supposed to play a key role in the mode of action of some potent drugs. In particular, $[Ru(NH_3)_5L]^{n+}$, where L is Cl^-, NH_3, or 4-picoline, was shown to form a $[Ru(NH_3)_5(GS)]^{2+}$ species under hypoxic conditions, protecting the cells from Ru binding to DNA.[57] Furthermore, Sadler et al. have shown quite recently that ruthenium compounds are able to form S bound adducts with methionine and cysteine in solution.[12a] In this study we provide further experimental evidence that sulfur-containing biomolecules can act as nitrogen-competing ligands for ruthenium-based drugs in general and for *trans*-$[RuCl_4(Hind)_2]^-$ in particular.

Final Remarks

Our results demonstrate that (i) the nitrogen atom N7 is a potential binding site for ruthenium(III) of *trans*-$[RuCl_4(Hind)_2]^-$ in both AMP and DNA, (ii) sulfur-donor ligands such as methionine should be regarded as potential nitrogen-competing ligands which may exert an effect on the metabolic transformation of *trans*-$[RuCl_4(Hind)_2]^-$ on its way to the cell DNA as the ultimate target, (iii) study of the thermodynamics and kinetics for the monofunctional binding of the complex *trans*-$[Ru^{III}Cl_4(Hind)_2]^-$ to the purine nucleobase N7 site and to sulfur-donor ligands is still required (computational studies are now underway in our laboratory), and (iv) it is also unclear whether it is the *trans*-$[Ru^{III}Cl_4(Hind)_2]^-$complex, the monoaqua species formed upon hydrolysis, or a ruthenium(II) species, activated by reduction, which plays the pivotal role for the antitumor activity. The isolation of aqua species and the study of their reactivity toward nucleobases and thioethers and further electrochemical studies will be of special concern in our future investigations.

The X-ray diffraction studies performed highlight the mode of binding of 9-methyladenine to *trans*-$[Ru^{III}Cl_4(Hind)_2]^-$ and the configuration of **2** and **3** as *trans*,*trans*,*trans*-$[Ru^{II}Cl_2(Hind)_2(R_2S)_2]$ isomers. In fact, the first crystallographic evidence for monofunctional binding of 9-substituted adenine to ruthenium via N7 is reported. As a final consideration, we note that compounds **1a**,**b** expand the relatively small class of Ru−nucleobase complexes characterized by X-ray diffraction methods.

Acknowledgment. We thank Prof. G. Giester for X-ray diffraction and Dr. M. Galanski for NMR measurements and Dr. Ch. Hartinger and Mr. W. Joppek for their assistance with mass spectrometry investigations. Prof. V. Yu. Kukushkin is acknowledged for helpful discussion.

Supporting Information Available: X-ray crystallographic CIF files for **1a**,**b**, **2**, and **5** and additional figures. This material is available free of charge via the Internet at http://pubs.acs.org.

IC048967H

(57) Frasca, D. R.; Clarke, M. J. *J. Am. Chem. Soc*. **1999**, *121*, 8523−8532.